LATE-STAGE INTRUSIVE ACTIVITY AT OLYMPUS MONS, MARS: SUMMIT INFLATION AND GIANT DIKE FORMATION

Peter J. Mouginis-Mark[1*] and Lionel Wilson[2]

[1]Hawaii Institute of Geophysics and Planetology
University of Hawaii
Honolulu, Hawaii 96822
USA

[2]Lancaster Environment Centre
Lancaster University
Lancaster LA1 4YQ
UK

Icarus

In press, September 2018

Keywords:

Mars
Olympus Mons
Ascraeus Mons
Volcanic dikes

Abstract

By mapping the distribution of 351 lava flows at the summit area of Olympus Mons volcano on Mars, and correlating these flows with the current topography from the Mars Orbiter Laser Altimeter (MOLA), we have identified numerous flows which appear to have moved uphill. This disparity is most clearly seen to the south of the caldera rim, where the elevation increases by >200 m along the apparent path of the flow. Additional present day topographic anomalies have been identified, including the tilting down towards the north of the floors of Apollo and Hermes Paterae within the caldera, and an elevation difference of >400 m between the northern and southern portions of the floor of Zeus Patera. We conclude that inflation of the southern flank after the eruption of the youngest lava flows is the most plausible explanation, which implies that intrusive activity at Olympus Mons continued towards the present beyond the age of the youngest paterae ~200 – 300 Myr (Neukum et al., 2004; Robbins et al., 2011). We propose that intrusion of lateral dikes to radial distances >2,000 km is linked to the formation of the individual paterae at Olympus Mons. Two specific dikes to the SE of the volcano are inferred to have volumes of ~4,400 km^3 and ~6,100 km^3, greater than the volumes of individual calderas and implying triggering of both caldera collapse and lateral dike injection by the arrival of large inputs of magma from the mantle. A comparable disparity between lava flow direction and current topography, together with a tilted part of the caldera floor, has been identified at Ascraeus Mons.

Introduction

The Martian volcano Olympus Mons (18.65˚N, 226.2˚E) possesses a summit caldera ~60 x 80 km in diameter comprising six overlapping collapse pits ("paterae"), and the geology of the volcano has been compared to that of volcanoes in Hawai'i (Carr, 1981; Hodges and Moore, 1994) and Nicaragua (Mouginis-Mark et al., 2007). Numerous lava flows originate from the caldera rim and extend to the lower flanks, and the vents for these flows are missing, presumed destroyed within the calderas following late-stage summit collapse (Mouginis-Mark, 1981; Mouginis-Mark and Robinson, 1992). Our comparison of lava flow directions with topographic data collected from the Mars Orbiter Laser Altimeter (MOLA) (Smith et al., 2001) reveals that flows on the southern rim of Olympus Mons caldera apparently travelled uphill. In addition, the highest point on the volcano is off-set from the center-of-figure of the shield. The high point on the volcano is >200 m higher than any point on the caldera rim crest, and >1,600 m higher than the northern caldera rim. While disparities between lava flow directions beyond the basal escarpment of Olympus Mons have previously been reported (Mouginis-Mark et al., 1982; Isherwood et al., 2013; Chadwick et al., 2015), this is the first time that such topographic and flow direction differences have been recognized close to the summit.

We contend that the emplacement of the lava flows predates the latest period of summit inflation at the volcano, indicating that the parent magma chamber remained molten, and continued to receive new magma from depth, after the latest episodes of caldera collapse. Here, we propose that caldera collapse may have been linked to the emplacement of lateral dikes extending to significant distances (in some instances >2,000 km) from Olympus Mons, and that the last phase of summit inflation was insufficient to initiate further dike intrusions. This suggests a minimum volume-limited threshold for dike emplacement and associated caldera collapse. Two candidate dikes are identified to the south and SE of Olympus Mons; these have calculated volumes comparable to that of the paterae but greater than the post-collapse inflation of the summit. These observations indicate that magmatism within the Tharsis region of Mars took place more recently than indicated by crater counts of the summit areas (Neukum et al., 2004; Robbins et al., 2011), perhaps as recently as <200 Myr. Supporting this idea, Hauber et al. (2011) have identified individual lava flows to the east of Olympus Mons and Pavonis Mons which may also be younger than 100 Myr. Cumulative size/frequency crater curves derived by Warner (2009; her Fig. 4) and Richardson et al. (2017) also suggest that some small flows on Arsia Mons may be comparably young. Our analysis of the summit areas of other Martian volcanoes reveals that comparable post-collapse inflation has taken place at Ascraeus Mons, but that the summit areas of other Tharsis volcanoes do not have this attribute.

Observations

We have mapped the distribution of lava flows at the summit of Olympus Mons, using images from the Context Camera (CTX) (Malin et al., 2007) and the High Resolution Imaging Science Experiment (HiRISE) (McEwen et al., 2007) instruments, which provide visible images with a spatial resolution of ~6 m/pixel and ~0.25 m/pixel, respectively. We have mapped 351 individual lava flows and lava channels at the summit of Olympus Mons (Fig. 1), of which 28 are truncated by the caldera rim. All of the mapped flows are >10 km in length, and are recognized either by the lobate edges of individual flow lobes or by a continuous central lava channel. No clear examples of vents can be identified for any of these flows, which leads us to support the idea that the flows originated within a summit area since destroyed by caldera collapse (Mouginis-Mark, 1981, 2017; Mouginis-Mark and Robinson, 1992).

Comparing topographic data from MOLA with the mapped lava flow locations (Fig. 1) reveals that there is a marked difference between the direction of flow and the maximum topographic gradient on the southern upper flank. Flows originating from the southern rim of Apollo Patera extend uphill by >200 m, crossing the contours at $\sim 90^{\circ}$ (Figs. 2 and 3). On the eastern rim, the flows parallel the contours. Only on the northern rims of Zeus and Athena Paterae do the flows cross the contours perpendicularly and travel downhill in the expected direction.

The floors of the Olympus Mons paterae are interpreted to be solidified lava lakes, or extensive individual lava flows which buried the talus produced during caldera collapse under a relatively thin veneer of fresh lava (Mouginis-Mark, 2017). We contend that soon after formation each patera floor would have been an equipotential surface, i.e., a locally horizontal surface. However, topographic profiles across the floors of Hermes and Apollo Paterae reveal that they are tilted towards the area of maximum elevation on the volcano by $\sim 1^{\circ}$ (Fig. 4). Apollo Patera is ~100 m higher on the SW floor compared to the NE floor, and Hermes Patera is ~320 m higher on the SW floor compared to the NE floor. Multiple wrinkle ridges on the floor of Hermes Patera appear to be consistent with post-formation uplift of the floor (most likely during several discrete episodes), while other ridges and graben within Zeus Patera may in part be due to “sagging” of the central portion of the floor (Zuber and Mouginis-Mark, 1992).

Additional evidence exists for changes in the topography of the caldera floor post-formation. The floor of Zeus Patera, which is the first and largest of the collapse features within the caldera, most likely formed a horizontal surface because it appears to have formed in a single event. However, present topography (Fig. 5) shows that the southern portion of the floor lies at an elevation ~400 m higher than the northern floor. Most of the circumferential graben on the floor (Zuber and Mouginis-Mark, 1992) lie below an elevation of 18.90 km on the northern portion and above this elevation on the southern floor. This suggests that either the southern floor was raised or, less likely, that the northern floor subsided by this amount. The simplest interpretation consistent with the disparity between lava flow directions and present topography is that the southern floor has been raised by ~400 m, with the foot of the southern wall of Zeus Patera at ~19.30 km elevation (Fig. 5). It is not possible to determine the relative timing of some of these tilting events. At least part of the ~400 m uplift of Zeus Patera could have taken place prior to the formation of Hermes or Apollo Paterae, as there is a pronounced sequence of events for the evolution of the caldera, with Zeus Patera the oldest (Mouginis-Mark, 2017).

In contrast, Athena Patera displays no obvious tilting of its floor (Fig. 6). The elevation of the floor varies from a high point of ~18.04 km and a low point of ~17.71 km. In general, the floor is higher around the perimeter, with a low dome (~100 m high) on the NE floor. The lack of clear evidence of tilting of the floor may be because Athena Patera lies further from the center of uplift, or it may indicate that this collapse pit is the youngest collapse event and formed after uplift had ceased. Stratigraphically, Athena Patera could be as old as any patera except Zeus Patera. Morphologic data are not available to resolve which explanation is more likely, but crater counts (Neukum et al., 2004; Robbins et al.,

2011) suggest that Athena Patera is one of the older collapse features. However, Mouginis-Mark (2017) showed that previous crater counts for the caldera are contaminated by secondary craters from the impact crater Pangboche, so that a direct crater-age comparison between Apollo and Athena Paterae is not possible.

A further test for the spatial extent of the inferred uplift comes from an inspection of the floor of the 10.4 km diameter Pangboche crater (Fig. 7), which lies <20 km from the highest point on the volcano. Ejecta from Pangboche crater extends across the floors of Apollo and Dionysus Paterae, so that the crater formed at some time after the latest episodes of caldera collapse (Mouginis-Mark, 2017). As documented by Mouginis-Mark (2015), there is a well-preserved deposit of impact melt on the floor of Pangboche crater. This melt most likely cooled as a single unit, and formed a horizontal surface. Inspection of a HiRISE-derived digital elevation model (Fig. 7) reveals that the eastern portion of this melt pond is horizontal, with ~5 m difference in elevation between the northern and southern portions of the floor. Thus, since the formation of Pangboche crater, there has been no further inflation of the summit.

Patera Formation

The lack of large-volume lava flows which have vents on the flanks of Olympus Mons (Mouginis-Mark, 2017), which might have caused incremental caldera collapse due to multiple flank eruptions, requires an alternative explanation for the initiation of caldera collapse. For example, Mouginis-Mark (2017) found no evidence for previously proposed flank vents on Olympus Mons (Peters and Christensen, 2017), concluding that changes in flank flow morphology are due to subtle differences in slope. The formation of nested calderas implies multiple collapse events each triggered by the partial evacuation of the subsurface magma chamber(s) with a change in volume per event ranging from ~412 to 3,675 km^3, with a total volume of 6,242 km^3 (Table 1). Subsidence of an evolving magma chamber into a lower zone of hot crustal rocks was proposed (Walker, 1988) as a viable mechanism leading to surface collapse at Hawaiian volcanoes, which may serve as a good terrestrial analog. At other volcanoes on Earth it is possible that unrecognized distal flank eruptions and intrusions during the caldera collapse event might explain magma loss from the summit region (Simkin and Howard, 1970; Sigurdsson and Spark, 1978).

Our model for the formation of the individual paterae within the Olympus Mons caldera is that each subsidence event was initiated by the intrusion of a large lateral dike extending to a great distance radial to the volcano. For a range of plausible model parameters (Zuber and Mouginis-Mark, 1992), the maximum depth to the top of the active magma chamber of Olympus Mons must have been <16 km. A simple magma chamber model consists of magma with density ρ_m filling a chamber with vertical height H centered at a neutral buoyancy level. This level is located at depth D below the surface between upper crustal rocks of density ρ_u and lower crustal rocks of density ρ_l, such that $\rho_l > \rho_m > \rho_u$. Neutral buoyancy requires that $(\rho_l - \rho_m) = (\rho_m - \rho_u)$. We adopt inferred magma density values (Rubin and Pollard, 1987) for Kilauea volcano, i.e., ρ_l, ρ_m and ρ_u equal to 2900, 2600 and 2300 kg m^{-3}, respectively, for which $(\rho_l - \rho_m) = (\rho_m - \rho_u) = \Delta\rho = 300$ kg m^{-3}. With this simple configuration, the excess magma pressure, ΔP, inside the chamber acting to fracture the chamber wall is a maximum at the chamber center-line at depth D and has the value $(0.5\ g\ H\ \Delta\rho)$ where g is the acceleration due to gravity, 3.711 m s^{-2}. If magma chambers commonly grow into a roughly spherical shape, then the 20 to 50 km diameters of the Olympus Mons summit paterae suggest that H could be at least 20 km, in which case ΔP would be at least 11 MPa. This value is of the same order as the expected tensile strengths of rocks (Roy et al., 1981) suggesting that the proposed model is plausible. With the top of the chamber at a depth of 16 km for Olympus Mons (Zuber and Mouginis-Mark, 1992) and a chamber height of 20 km, dikes leaving the chamber would have propagated laterally from its mid-line at a depth of at least 26 km (i.e., $16 + 0.5 \times 20$ km) below the volcano summit, i.e., at least ~4 km below the mean surface level surrounding the volcano.

We have searched for large graben radial to Olympus Mons which would be the surface traces of large dikes. We speculate that each collapse event which formed a patera within the caldera was connected with a lateral dike intrusion, but of course cannot correlate a specific dike with a specific collapse event. Two clear candidate dikes exist to the SE, namely Aganippe Fossa (7º00’S, 233º40’E), extending to ~1,710 km from the center of the caldera, and a graben in Phoenicis Lacus (13º00’S, 249º40’E) extending to ~2,530 km from the caldera (Fig. 8). Aganippe Fossa is ~425 km long and lacks discrete pits, but the bounding graben walls are ~3 to 7 km apart. Other, unidentified, dikes are postulated to have been linked to the formation of the other paterae. Numerous fractures within Ulysses Fossae (12ºN, 237ºE) are radial to Olympus Mons, and thus might be the surface manifestations of dikes related to caldera collapse episodes. The surface expression of the Phoenicis Lacus graben extends for ~185 km and comprises a series of connected rimless pits ~4 km in diameter, with bounding graben walls (Fig. 9). The width and depth of each graben was measured (using CTX images and MOLA topography, respectively), at a series of locations as shown in Fig. 8 and these geometric data are given in Table 2. The general trend with increasing distance from Olympus Mons is for the broad depression of the Phoenicus graben to narrow and then break into a series of coalescing pits, and final individual pits. This is consistent with observations of the collapse features associated with the dike system approaching the surface along the East Rift Zone of Kilauea volcano, Hawai‘i (Okubo and Martel, 1998).

The values in parentheses in Table 2 are locations where the grabens are anomalously wide, possibly due to magma withdrawal and surface subsidence or localized minor explosive activity. Ignoring these locations, as measured at the surface, the average depth and width of the Aganippe graben are 345 m and 7.5 km, respectively. The corresponding values for the Phoenicis graben are 320 m and 4.2 km. Based on measurements of two dike-induced graben in Iceland (Rubin, 1992), the ratio (graben width) / (depth to dike top) (Wilson and Head, 2002) is on average 3.5 and the ratio (dike width) / (vertical subsidence of graben floor) is 1.25. Using these ratios, we find that the Aganippe dike was ~430 m wide with its top at a depth of 2.1 km below the surface and that the Phoenicis dike was 400 m wide with its top 1.2 km deep.

We noted above that any radial dike leaving a magma chamber inside Olympus Mons probably had its center at a depth of at least 4 km below the general planetary surface level. At the locations of the graben, our measurements imply that the dike tops were at a depth of 1 km to 2 km. This suggests that the half-heights of the dikes were at least ~3 km. Multiplying total dike heights of 6 km by the above estimated widths and the extents of the dikes from Olympus Mons we find minimum magma volumes in the dikes of 4,400 km^3 for Aganippe and 6,070 km^3 for Phoenicis, a total of at least ~10,500 km^3.

The waning phase of activity at Olympus Mons was evidently characterized by the cessation of the eruption of lava flows from vents at the summit followed by caldera collapse events linked to the propagation of large lateral dikes able to extend a few thousand kilometers from the volcano. Because the volumes of the lateral dikes are greater than that of even the largest patera, it seems probable that magma must have been “buffered” within the edifice (Parfitt and Head, 1993; Parfitt et al., 1993). It is also likely that any magma chamber was only partially emptied. This dike intrusion could occur at the end of the life of a magma chamber when the arrival of an unusually large dike rising from the mantle inflated the magma chamber to the point where multiple ruptures occur. Not only is a lateral dike initiated, but also the stresses on the overlying rocks cause caldera collapse to begin. The volume of magma intruded into the lateral dike consists of contributions from both the caldera subsidence and the new mantle magma. Multiple episodes of this kind of activity occurred at Olympus Mons, with the latest collapse occurring ~200 – 300 Myr ago (Neukum et al., 2004; Robbins et al., 2011). There are insufficient topographic and morphologic data to resolve if inflation preceded each caldera collapse event, or if the difference in lava flow direction and present topography is due to the single most recent event or to multiple smaller inflation events. Thus, some of the 400 m uplift of the southern floor of Zeus Patera may be a relic of an earlier inflation event which ultimately produced a younger patera (such as Apollo Patera).

It is not easy to compare the volume of each dike with the volume of the inflated area at the summit of Olympus Mons, primarily because the horizontal extent of this uplift is not clear. If all of the uplift resulted from a single event (rather than multiple episodes of inflation followed by caldera collapse), then the horizontal extent of uplift could reasonably be defined by the 20.0 km contour on the volcano (Fig. 1). This contour defines an approximate width of inflation as 100 km. Taking the maximum elevation of the southern rim (i.e., ~21.20 km) as the center of uplift, and approximating the shape of the uplift as a cone, this would imply a volume of ~3,150 km^3. This volume is ~50% to 70% the inferred volume of the lateral dikes that we have identified, and so would be consistent with the inability of the last inflation event to drive a new episode of dike intrusion.

The following sequence of events at Olympus Mons can be inferred from the distribution of flows and the topography of the paterae floors: 1. The paleo-summit began as a topographic high that lacked a caldera complex. 2. Lava flows erupted from this summit area, and extended down the flanks of the volcano. 3. Successive collapses of Zeus, Hera, Hermes and Dionysus Paterae took place, most likely linked with lateral dike intrusions which, by virtue of their inferred volumes, extended more than 1,000 km from the summit. The lava flows at the caldera rim were truncated and the vents were destroyed. 4. Inflation south of the summit began, tilting the floor of Zeus and Hermes Paterae. 5. Collapse of Apollo Patera took place due to a later phase of distal dike intrusion. 6. Inflation south of the caldera continued, tilting the floor of Apollo Patera, and continuing to tilt the floor of Hermes Patera. 7. Pangboche crater formed after the summit inflation had ceased.

Topography of Other Martian Volcanoes

Results comparable to Olympus Mons have been found for the summit of Ascraeus Mons (Fig. 10), where our mapping has identified 126 individual lava flows. Here the mismatch between flow direction and present day topography is greatest on the northern rim of the caldera, where truncated flows are evident on the rim (Mouginis-Mark and Rowland, 2001; Mouginis-Mark and Christensen, 2005). Examples of lava flows which now go uphill, or parallel the present contours, can be identified (Fig. 11). The total height difference across this summit area north of the caldera rim is ~100 m. At Ascraeus Mons, there appears to have been tilting of at least one of the paterae (not named) on the northern side of the caldera. The patera is proximal to the highest point on the volcano, and is ~300 m higher on its northern floor compared with the southern floor (Fig. 12). This appears to have been true tilting of the floor, rather than subsidence of the center of the patera, as the slope extends across the entire floor and the tilting is radial to the high-point. Inspection of the largest patera at the middle of the Ascraeus Mons caldera, which is the youngest of the collapse events (Mouginis-Mark, 1981), reveals no comparable tilting. We have performed a search for graben radial to Ascraeus Mons to explain the origin of the caldera. Numerous fractures which are sub-radial to Ascraeus Mons can be found within Tractus Catena (25°00'N, 257°00'E) to the north of the volcano, and within Uranius Fossae (23°10'N, 268°30'E) to the NE. However, the complex history of tectonic stresses in these areas makes it difficult to associate these features unambiguously with Ascraeus Mons.

Although we have found this topographic disparity at two of the Tharsis volcanoes, a review of lava flow distributions and MOLA topography reveals that there is no comparable evidence for late-stage summit inflation at either Pavonis or Arsia Montes. A possible explanation could be that these two volcanoes have lower maximum elevations, ~17.6 km at the western and southern rims of Arsia Mons and ~14.0 km on the southern rim of Pavonis Mons, compared with 18.2 km for Ascraeus Mons and ~21.2 km for Olympus Mons. Other attributes of each volcano may also come into play. For example, regional extensional tectonics more easily facilitating the intrusion of large dikes, as at Ceraunius Fossae south of Alba Mons, may have promoted the formation of nested calderas on Alba Mons (Mouginis-Mark et al., 1988; Schneeberger and Pieri, 1991; Ivanov and Head, 2006) at lower elevations. We note that the highest elevation on Alba Mons (~6.80 km) lies to the west of the caldera rim, with a dome ~300 m high located in the western rim of the volcano (McGovern et al., 2001), and that the mapped distribution of lava flows (Crown et al., 2017) is suggestive of late-stage inflation. Late-stage inflation of the western flank of Alba Mons may also explain the mismatch between the predicted dike orientations from doming centered on the calderas (Cailleau et al., 2005).

Elysium Mons (maximum rim elevation ~14.0 km on the northern and southern rims) has a caldera floor tilted down towards the east, but no lava flows can be identified at the summit. Tilting of an old portion of the caldera floor at Apollinaris Mons (rim elevation ~3.5 km) has previously been identified (Robinson et al., 1993), but again the lack of recognizable lava flows precludes a comparison of flow directions and topography. Albor Mons (rim elevation ~3.9 km on the southern rim) displays caldera floor topography consistent with the sagging of the central portion, with the perimeter ~600 m higher than the center of the caldera. Similarly, the central portion of the floor of Uranius Mons (rim elevation ~2.3 km) is ~500 m lower than the perimeter. We leave to a future investigation an analysis of how a particular volcano may experience summit inflation, the formation of large-volume radial dikes, and how these attributes may relate to the neutral density level of the magma chamber (Wilson and Head, 2002; Scott et al., 2002).

Conclusions

Our observations of the summits of Olympus and Ascraeus Montes imply that igneous activity on Mars continued closer towards the present day than previously inferred from crater counting of the geological units on the caldera floors (Neukum et al., 2004; Robbins et al., 2011). If the Phoenicus graben and Aganippe Fossa are indeed the surface manifestation of dikes from Olympus Mons, then it is possible that the influence of an individual volcano may extend to thousands of kilometers from the construct. Such a conclusion is consistent with the idea that a giant dike from Arsia Mons initiated the outflow of water which formed Mangala Vallis (Wilson and Head, 2004), and that large dikes from Elysium Mons could have been responsible for the formation of Hrad Vallis (Wilson and Mouginis-Mark, 2003).

It is evident that the magma chambers within Olympus and Ascraeus Montes were fed with new magma from the mantle after the floors of the summit calderas were created, causing each chamber to inflate. The duration of these inflation events cannot be resolved, but potentially collecting age dates (through detailed crater counting of high-resolution images) for the surface expressions of the radial dikes might provide such information. Such analyses would be important for estimating the timing of this last phase of igneous activity, but await a future investigation.

Acknowledgements

This work results from detailed geologic mapping of Olympus Mons under NASA grant NNG05GH51G. LW acknowledges support from the Leverhulme Trust via an Emeritus Fellowship. We thank Harold Garbeil for the production of the digital elevation model presented in Figure 7, and two anonymous reviewers for their constructive comments on earlier versions of this manuscript.

References

Cailleau, B., Walter, T. R., Janle, P., Hauber, E., 2005. Unveiling the origin of radial grabens on Alba Patera volcano by finite element modelling. Icarus 176, 44 -56.

Carr, M. H., 1981. The surface of Mars. Yale University Press, pp. 87 – 110.

Chadwick, J., McGovern, P., Simpson, M., Reeves, A., 2015. Late Amazonian subsidence and magmatism of Olympus Mons. J. Geophys. Res. 120, doi:10.1002/2015JE004875.

Crown, D. A., Berman, D. C., Platz, T., Svheidt, S. P., Hauber, E., Weitz, C. M., 2017. Geologic mapping of the summit and western flank of Alba Mons, Mars. 3rd Planetary data Workshop 2017, LPI Contr. 1986.

Hauber, E., Broz, P., Jagert, F., P. Jodlowski, Platz, T., 2011. Very recent and wide-spread basaltic volcanism on Mars. Geophys. Res. Lttrs. 38, L10201, doi: 10.1029/2011GL0473110.

Hodges, C. A., Moore, H. J., 1994. Atlas of volcanic landforms on Mars. U.S. Geological Survey Prof. Paper 1534.

Isherwood, R. J., Jozwiak, L. M., Jansen, J. C., Andrews-Hanna, J. C., 2013. The volcanic history of Olympus Mons from paleo-topography and flexural modeling. Earth Planet. Sci. Lttrs. 363, 88 – 96.

Ivanov, M. A., Head, J. W., 2006. Alba Patera, Mars: Topography, structure, and evolution of a unique late Hesperian-early Amazonian shield volcano. J. Geophys. Res. 111 (E9), doi: 10.1029/2005JE002469.

Malin, M. C. and 13 others, 2007. Context Camera investigation on board the Mars Reconnaissance Orbiter. J. Geophys. Res. 112 (E5), doi: 10.1029/2006JE002808.

McEwen, A. S. and 14 others, 2007. Mars Reconnaissance Orbiter's High Resolution Imaging Science Experiment (HiRISE). J. Geophys. Res. 112 (E5), doi: 10.1029/2005JE002605.

McGovern, P. J., Solomon, S. C., Head, J. W., Smith, D. E., Zuber, M. T., Neumann, G. A., 2001. Extension and uplift at Alba Patera, Mars: Insights from MOLA observations and loading models. J. Geophys. Res. 106 (no. E10), 23,769 – 23,809.

Mouginis-Mark, P. J., 1981. Late-stage summit activity of martian shield volcanoes. Proc. Lunar Planet. Conf. 12th, p. 1431-1447.

Mouginis-Mark, P. J., 2015. Cratering on Mars with almost no atmosphere or volatiles: Pangboche crater. Meteoritics Planet. Sci. 50 (1), 51 – 62.

Mouginis-Mark, P. J., 2017. Olympus Mons volcano, Mars: A photogeologic view and new insights. Chemie der Erde, https://doi.org/10.1016/j.chemer.2017.11.006.

Mouginis-Mark, P. J., Christensen, P. R., 2005. New observations of volcanic features on Mars from the THEMIS instrument. J. Geophys. Res. 110 (E08), doi:10/1029/2005JE002421.

Mouginis-Mark, P. J., Robinson, M., 1992. Evolution of the Olympus Mons caldera, Mars. Bull. Volcanol. 54, 347 – 360.

Mouginis-Mark, P. J., Rowland, S. K., 2001. The geomorphology of planetary calderas. Geomorphology, 37, 201–223.

Mouginis-Mark, P. J., Harris, A. J. L., Rowland, S. K., 2007. Terrestrial analogs to the calderas of the Tharsis volcanoes of Mars: in: The Geology of Mars: Evidence from Earth-based Analogs, ed. M. Chapman, Cambridge University Press, p. 71 – 94.

Mouginis-Mark, P. J., Wilson, L., Zimbelman J. R., 1988. Polygenic eruptions on Alba Patera, Mars. Bull. Volcanol. 50 (6), 361 – 379.

Mouginis-Mark, P. J., Zisk, S. H., Downs, G. S., 1982. Ancient and modern slopes in the Tharsis region of Mars. Nature 297, 546 – 550.

Neukum, G., Jaumann, J., Hoffmann, H., Head, J. W., Basilevsky, A. T., Ivanov, B. A., Werner, S. C., van Gasselt, S., Murray, J. B., McCord, T., and the HRSC Co-Investigator Team, 2004. Recent and episodic volcanic and glacial activity on Mars revealed by the High Resolution Stereo Camera. Nature 432, 971 – 979.

Okubo, C. H., Martel, S. J., 1998. Pit crater formation on Kilauea volcano, Hawaii. J. Volcanol. Geotherm. Res. 86, 1 – 18.

Parfitt, E. A., Head, J. W. (1993). Buffered and unbuffered dike emplacement on Earth and Venus: Implications for magma reservoir size, depth, and rate of magma replenishment. Earth, Moon, Planets, 61 (3) 249 – 281.

Parfitt, E. A., Wilson, L., Head, J. W. (1993). Basaltic magma reservoirs: factors controlling their rupture characteristics and evolution. J. Volcanol. Geotherm. Res. 55 (1-2), 1 – 14.

Peters, S. I., Christensen, P. R., 2017. Flank vents and graben as indicators of Late Amazonian volcano tectonic activity on Olympus Mons. J. Geophys. Res. 122 (3), 501 – 523, doi:10.1002/2016JE005108.

Richardson, J. A., Wilson, J. A., Connor, C. B., Bleacher, J. E., Kiyosugi, K., 2017. Recurrence rate and magma effusion rate for the latest volcanism on Arsia Mons, Mars. Earth Planet. Sci. Lttr. 458, 170 -178.

Robbins, S. J., Di Achille, G., Hynek, B. M., 2011. The volcanic history of Mars: High-resolution crater-based studies of the calderas of 20 volcanoes. Icarus 211, 1179 – 1203.

Robinson, M. S., Mouginis-Mark, P. J., Zimbelman, J. R., Wu, S. S. C., Ablin, K. K., Howington-Kraus, A. E., 1993. Chronology, eruption duration, and atmospheric contribution of the Martian volcano Apollinaris Patera. Icarus 104, 301 – 323.

Roy, R. F., Beck, A. E., Touloukian, Y.S., 1981. Thermophysical properties of rocks. In: Y. S. Touloukian, W. R. Judd and R. F. Roy (Eds), Physical Properties of Rocks and Minerals. McGraw-Hill, New York, 409-502.

Rubin, A. M., 1992. Dike-induced faulting and graben subsidence in volcanic rift zones. J. Geophys. Res. 97, 1839–1858.

Rubin, A. M., Pollard D. D., 1987. Origin of blade-like dikes in volcanic rift zones In Volcanism in Hawaii. (R. W. Decker, T. L. Wright, & P. H. Stauffer, Eds), U.S. Geol. Surv. Prof. Paper 1350, 1449–1470.

Schneeberger, D. M., Pieri, D. C., 1991. Geomorphology and stratigraphy of Alba Patera, Mars. J. Geophys. Res. 96 (B2), 1907 – 1930.

Scott, E. D., Wilson, L., Head, J. W., 2002. Emplacement of giant radial dikes in the northern Tharsis region of Mars. J. Geophys. Res. 107 (E4), p. 3-1 to 3-10, doi: 10.1029/2000JE001431.

Sigurdsson, H., Sparks, S. R. J., 1978. Lateral magma flow within rifted Icelandic crust. Nature 274, 126 – 130.

Simkin, T., K., Howard, A., 1970. Caldera collapse in the Galapagos Islands, 1968. Science 169 (3944), 429 – 437.

Smith, D. E. and 23 others, 2001. Mars Orbiter Laser Altimeter: experiment summary after the first year of global mapping of Mars. J. Geophys. Res. 106, 23,689 - 23,722.

Walker, G. P. L., 1988. Three Hawaiian calderas: an origin through loading by shallow intrusion. J. Geophys. Res. 93 (B12), 14,773 – 14,784.

Warner, S. C. (2009). The global martian volcanic evolutionary history. Icarus 201, 44 – 68.

Wilson, L., Head, J.W., 2002. Tharsis-radial graben systems as the surface manifestation of plume-related dike intrusion complexes: Models and implications. J. Geophys. Res. 107 (E8), doi:10.1029/2001JE001593.

Wilson, L., Head, J. W., 2004. Evidence for a massive phreatomagmatic eruption in the initial stages of formation of the Mangala Valles outflow channel, Mars. Geophys. Res. Lttrs. 31 (15), doi:10.1029/2004GL020322.

Zuber, M. T., Mouginis-Mark, P. J., 1992. Caldera subsidence and the magma chamber depth of the Olympus Mons volcano, Mars. J. Geophys. Res. 97 (E11), 18295 – 18307.

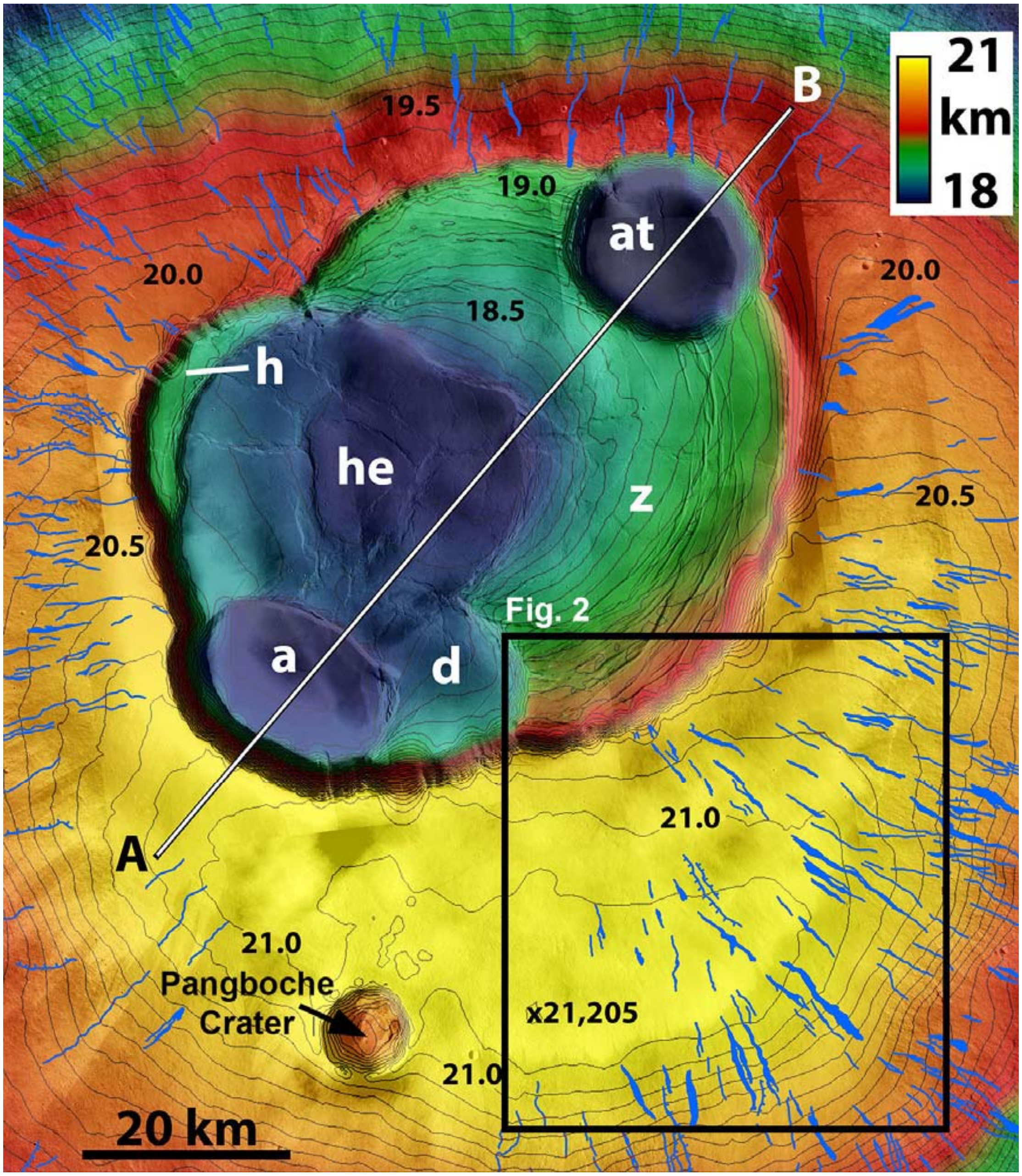

Figure 1: Topography of the summit of Olympus Mons. Contour interval is 100 meters, and are labeled in kilometers relative to Mars datum (Smith et al., 2001). Lava channels and lava flow lobes shown by blue lines, and are hachured where only the flow edge can be identified. Note that the highest elevation (21,205 m) lies to the south of the rim. Box denotes area shown in Fig. 2. Six paterae are identified by lowercase letters ("a" Apollo; "at" – Athena; "d" – Dionysus; "he" – Hermes; "h" – Hera; "z" – Zeus). The location of the profile in Fig. 4 is identified by line A to B. Base image is a mosaic of CTX frames.

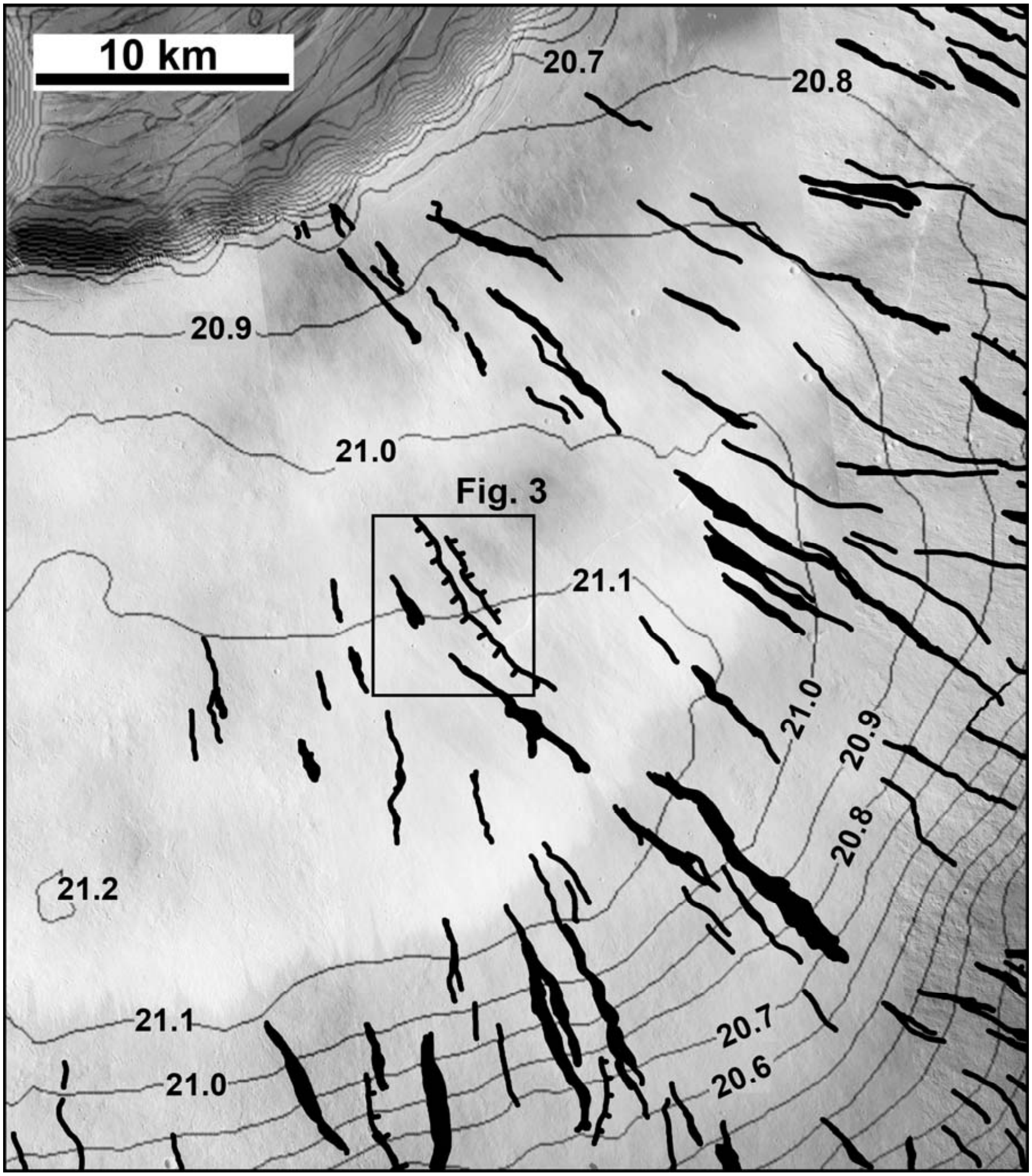

Figure 2: Details of lava flows (solid black, except where only the margins can be identified and shown as hachured lines) on SE flank with respect to local topography. Box denotes area shown in Fig. 3. Contour interval is 100 m, and heights are shown in kilometers. See Fig. 1 for location.

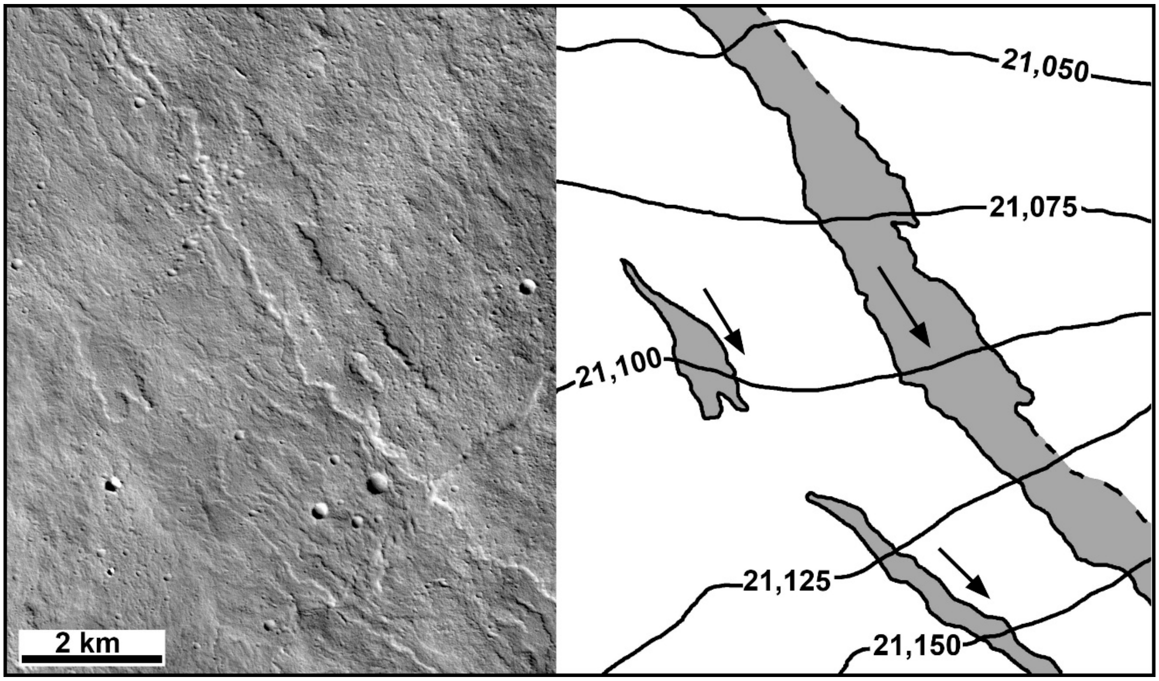

Figure 3: Details of flank topography south of the Olympus Mons caldera rim. At left is CTX image B08_012719_1986. At right, is an interpretative sketch of this area. Shaded areas are individual lava flows with dashed line denoting the inferred edge, and arrows denote direction of flow. See Fig. 2 for location. Contour interval is 25 m, and elevations are in meters.

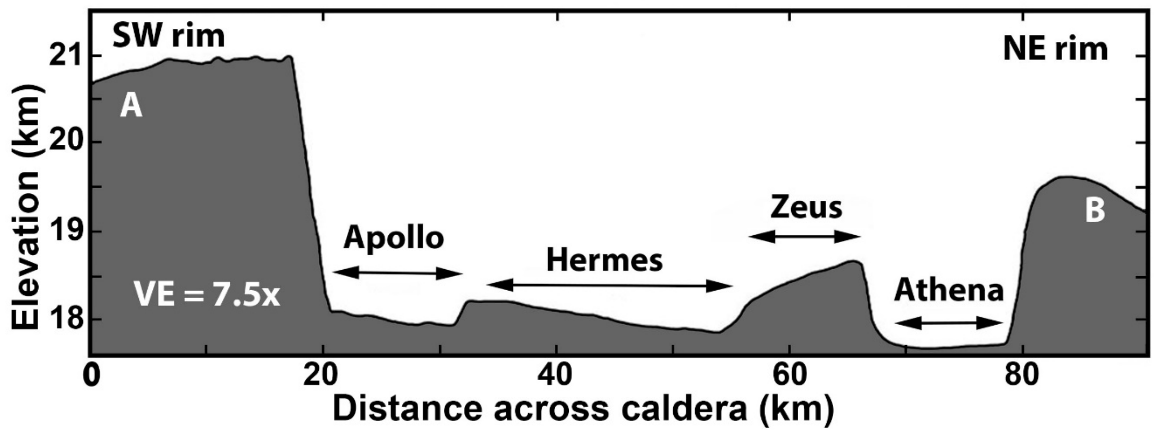

Fig. 4: Topographic profile across the floor of Olympus Mons caldera, adapted from Mouginis-Mark (2017). Profile derived from MOLA topographic data. See Fig. 1 for location. The floors of Apollo and Hermes Paterae are tilted upwards towards the highest point on the volcano summit at left of profile. In contrast, Athena Patera is essentially horizontal. The slope of Zeus Patera is interpreted to be due to the central sagging of this patera during an early phase of magma chamber evacuation (Zuber and Mouginis-Mark, 1992).

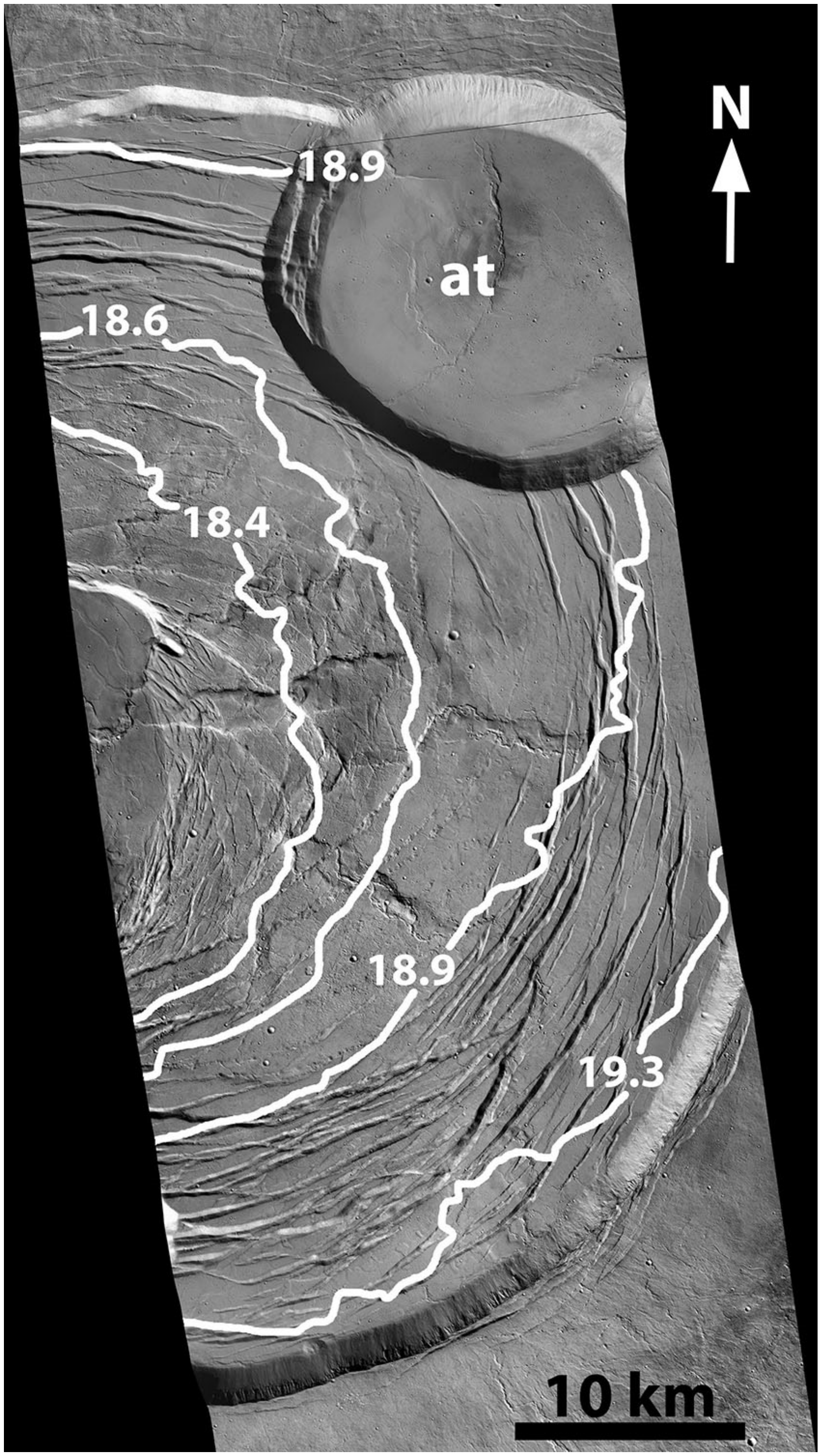

Figure 5: Topography of the floor of Zeus Patera within the summit caldera. Four contours (18.4 km, 18.6 km, 18.9 km and 19.3 km) are illustrated, showing that the SE portion of the floor of Zeus Patera lies at a much higher elevation than the NW floor of the same part of the caldera. “at” is Athena Patera. Base image is CTX frame B08_012864_1986.

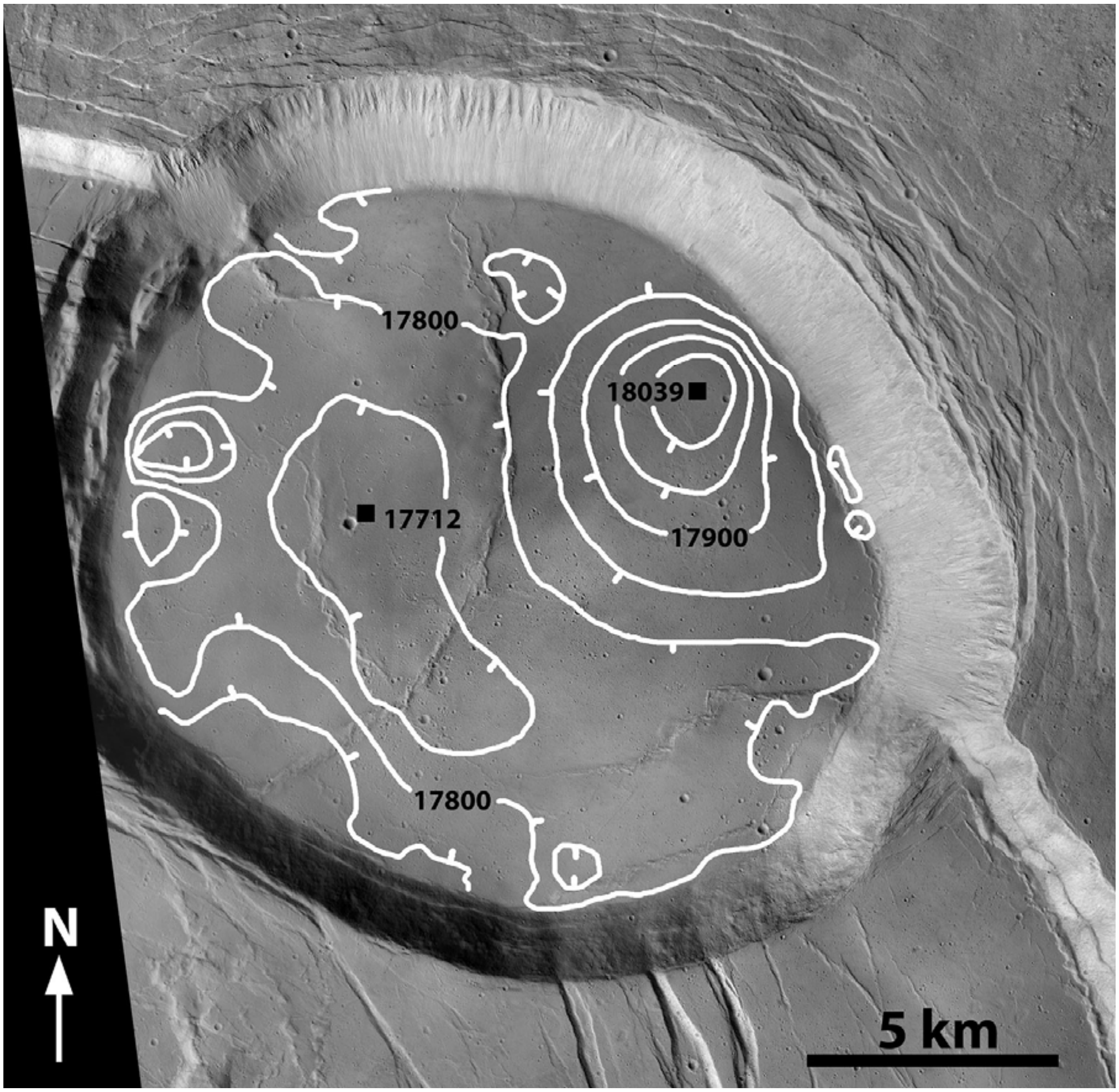

Figure 6: Topography of the floor of Athena Patera, illustrating that there is no clear tilting of the floor, although there is a ~100 m high dome on the NE part of the floor. Contour interval is 50 m, with the highest and lowest points (in meters) identified. Tick marks denote the downslope direction of closed contours. CTX image J06_047228_1985.

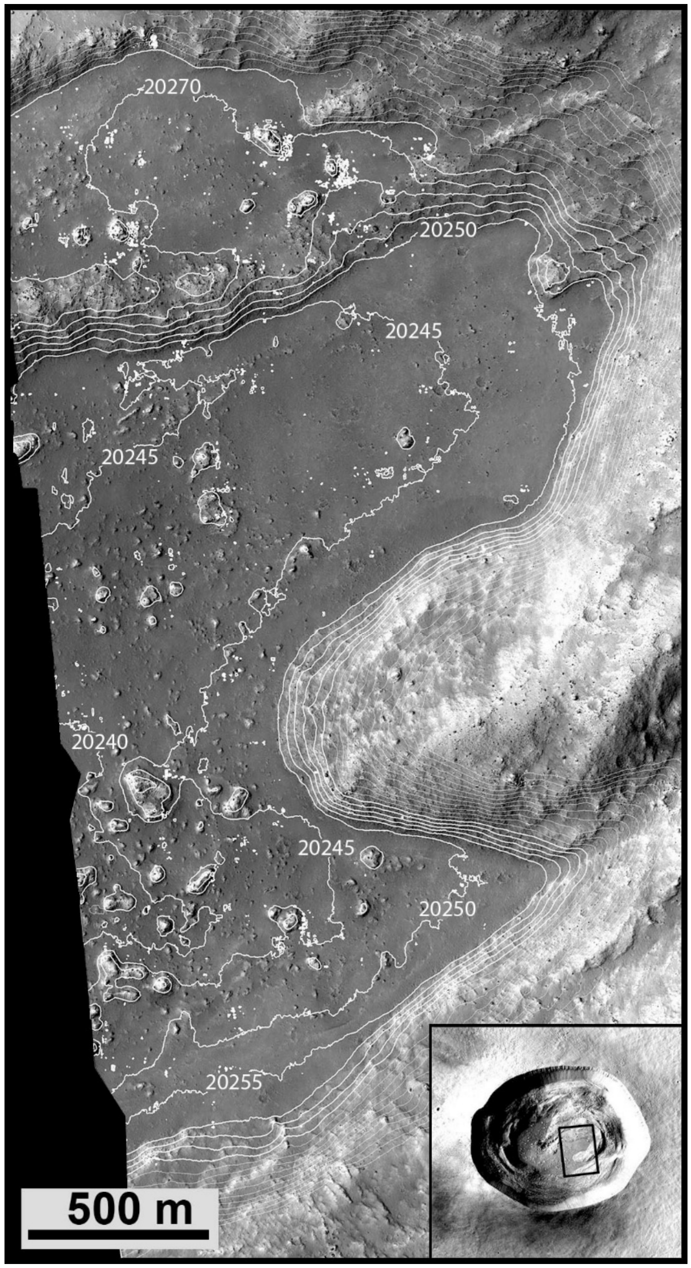

Figure 7: Topography of the floor of Pangboche crater, just to the south of the area of maximum uplift at Olympus Mons (see Fig. 1 for location). Contour interval is 5 m, derived by Harold Garbeil from digital elevation model produced from HiRISE images ESP_026024_1975 and ESP_026169_1975. The floor is virtually flat, showing no tilting at all, which implies that either Pangboche formed after the summit inflation ceased or that the crater formed on part of the flank which did not experience inflation. Given the fact that ejecta from Pangboche extends across Apollo Patera (Mouginis-Mark, 2017), the former explanation seems more likely. Insert at lower right shows location on the floor, and is part of CTX image P02_001643_1974.

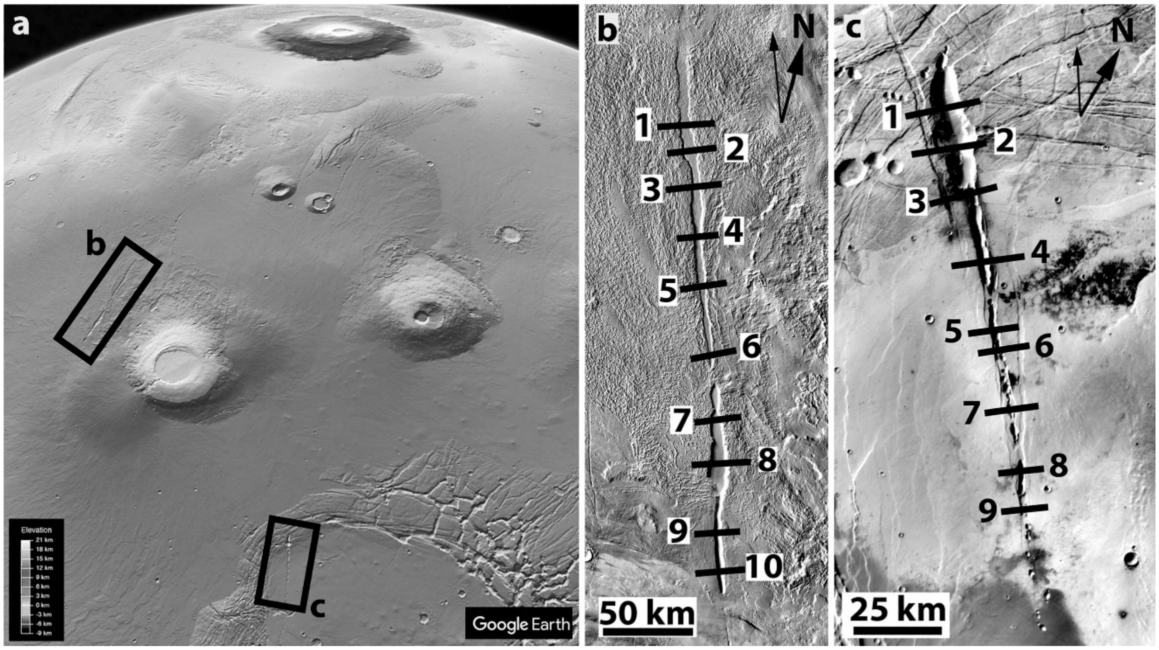

Figure 8: Locations of potential radial dikes associated with Olympus Mons. (a) Oblique view, looking northwest, with Olympus Mons at top center. Location of Figs. 8b and 8c indicated. Base image is a grey-scale elevation model derived from MOLA measurements. (b) Aganippe Fossa (7º 00'S, 233º40'E), which outcrops ~1,440 km to 1,710 km from the center of Olympus Mons caldera. Profiles included in Table 1 are numbered, small arrow (top right) points to Olympus Mons. CTX image G02_019312_1699. (c) Graben within Phoenicis Lacus (13º00'S, 233º40'E), ~2,200 km to 2,530 km from the caldera. Profiles included in Table 1 are numbered, small arrow (top right) points along a great circle to Olympus Mons. CTX image B22_018217_1659.

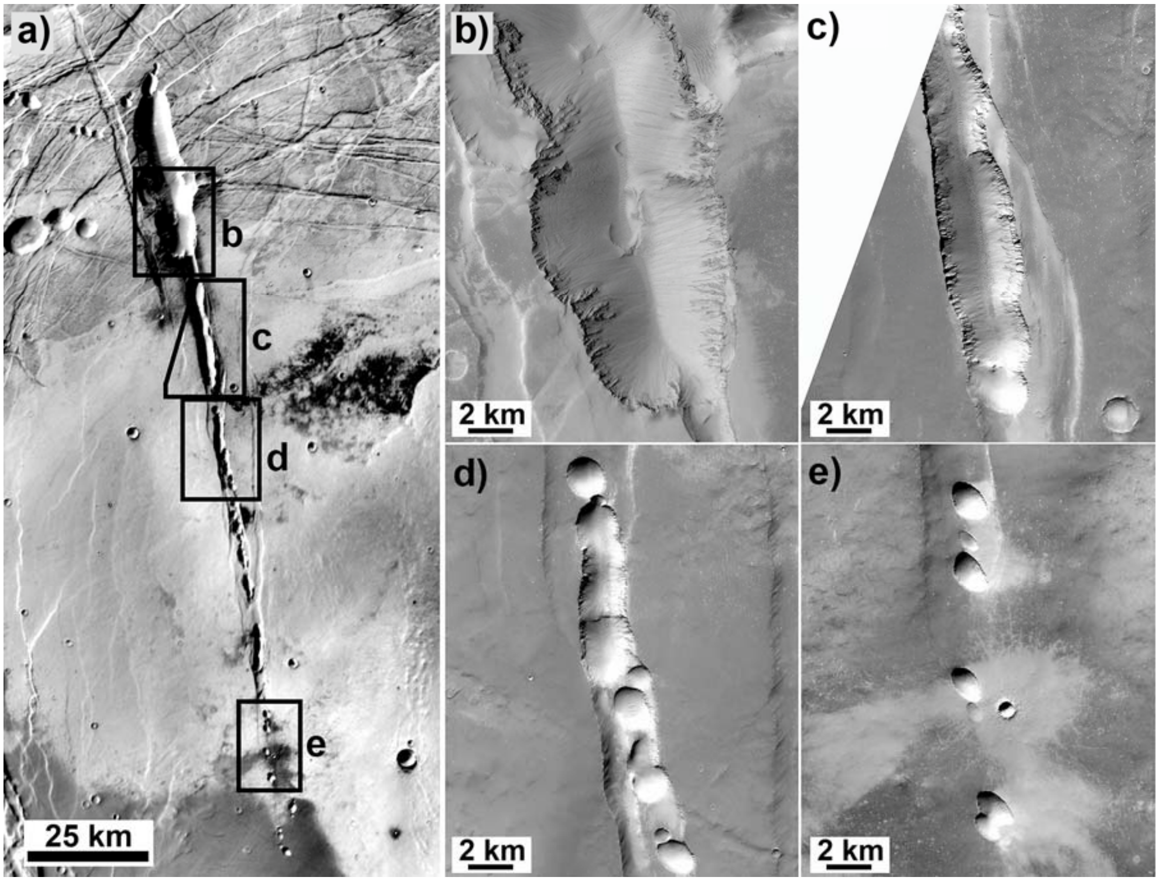

Figure 9: Details along Phoenicis graben. Notice that no indications of the top of the dike are visible within the graben or craters along the exposed length of the feature. Images are (a) THEMIS daytime IR mosaic; (b) CTX frame B11_013971_1676; (c) and (d) CTX frame B22_018217_1659; (e) CTX frame P06_003317_1653.

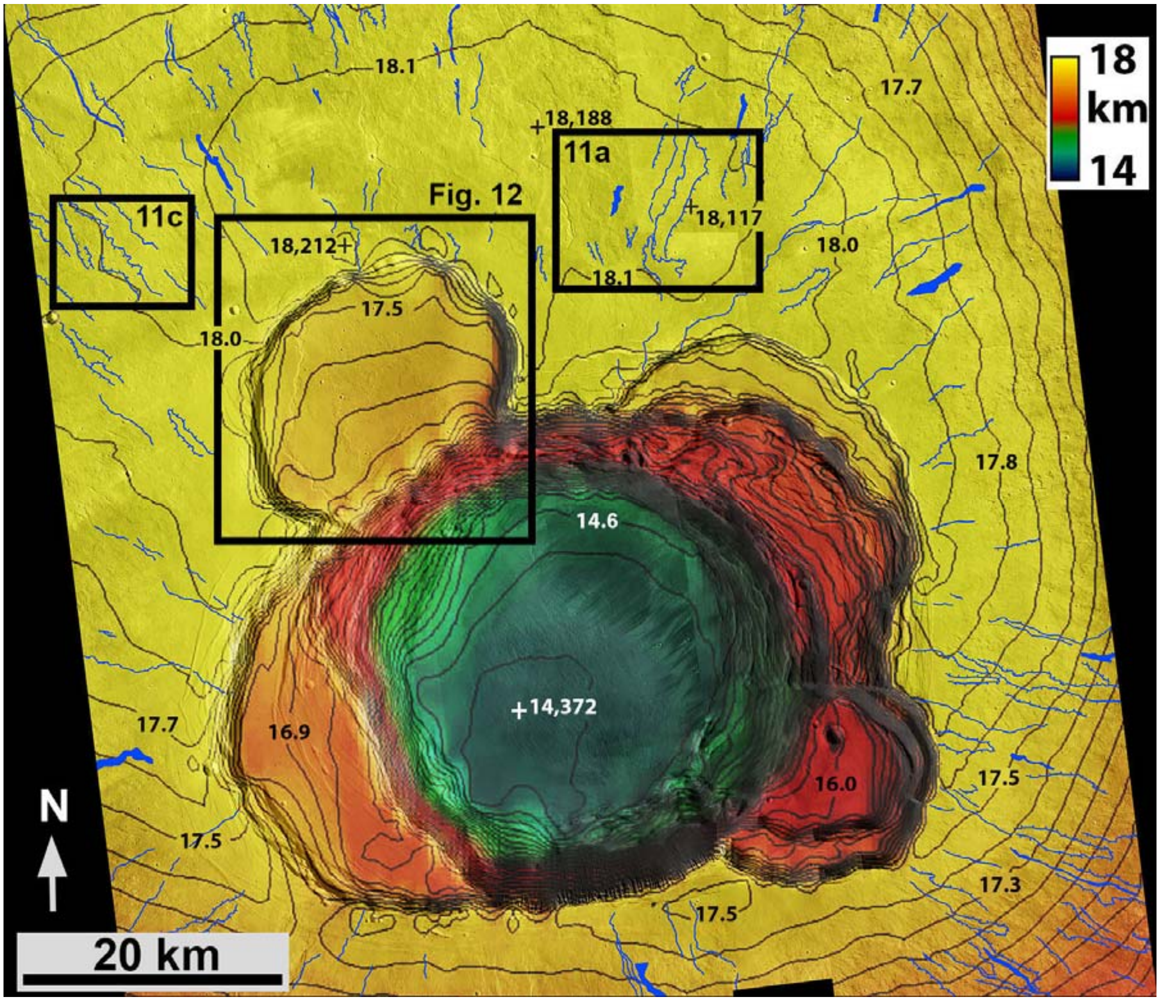

Figure 10: Topography and distribution of mapped lava flows at the summit of Ascraeus Mons. Note that the flows (hachured where only the flow edge can be identified) on the southern rim are perpendicular to the contours and go downhill, indicating no late-stage inflation here. The highest points (18,212 m, 18,188 m and 18,117 m) are identified on the north rim. Boxes mark the locations of Figs. 11a, 11c, and 12. Contour interval is 100 m, with the lowest point on the caldera floor (14,372 m) indicated. Base image is a mosaic of CTX frames.

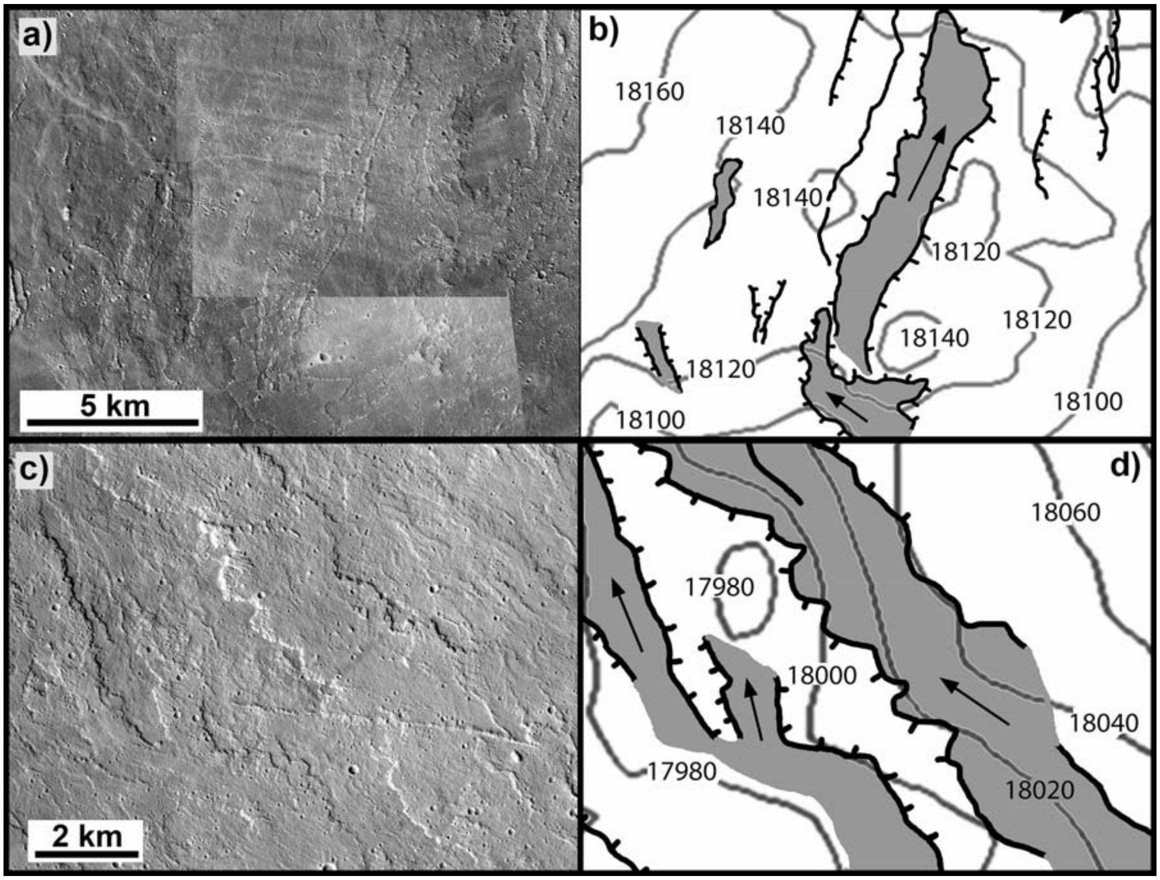

Figure 11: Details of two areas ("a" and "c") on the northern flank of Ascraeus Mons, showing disparity between lava flow directions and the local topography ("b" and "d"). Arrows in "b" and "d" show direction of flow. Contours in meters. See Fig. 10 for locations. Flows margins are hachured where the flow edge can be identified. a) is CTX frame P09_004398_1913; c) is CTX frame B06_012006_1912.

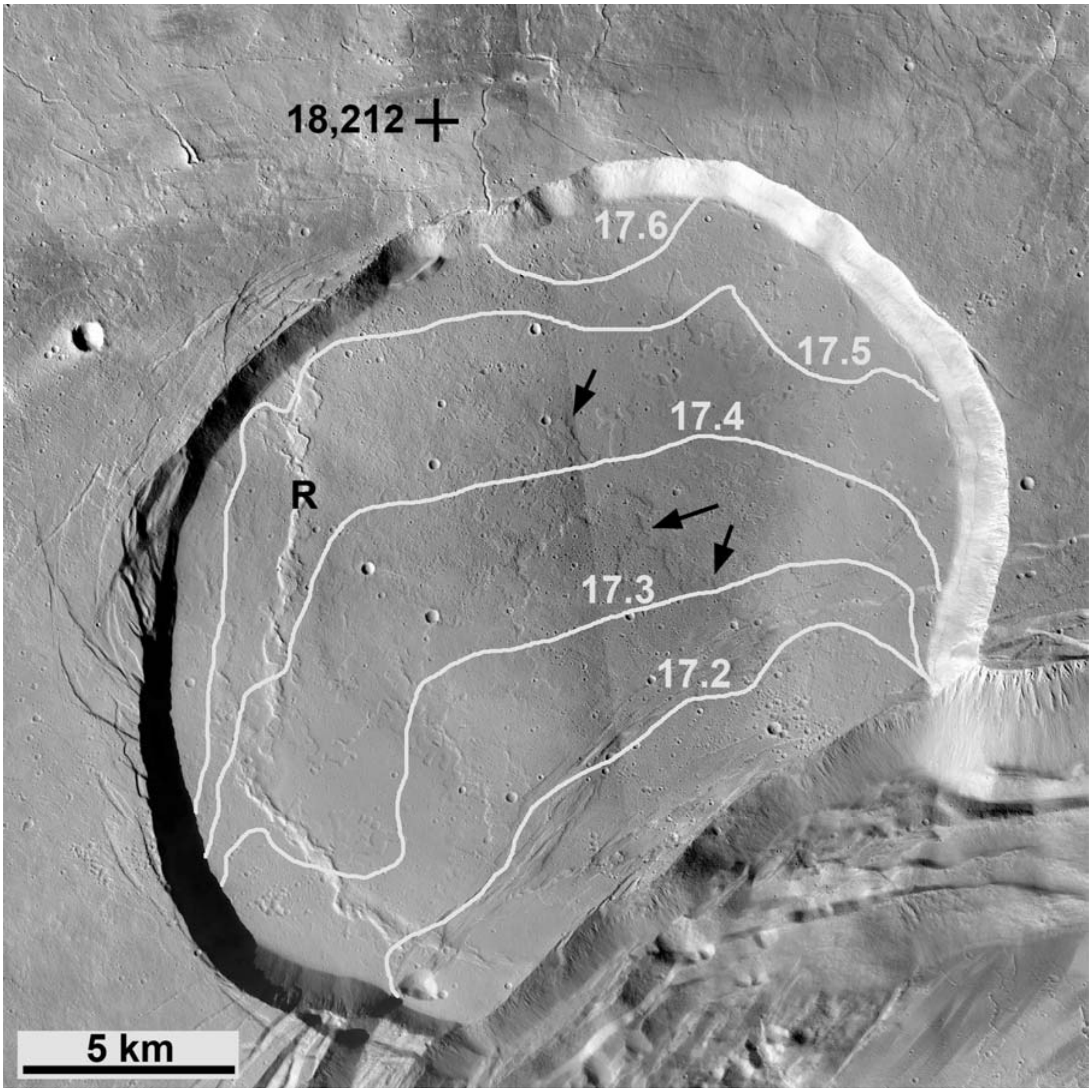

Figure 12: Details of the topography of the floor of the NW patera at the summit of Ascraeus Mons, which is presumed to have formed as a flat surface, only to be subsequently tilted towards the south by more than 500 m. Note that the slope of the patera is radial to the highest elevation on the volcano (18,212 m). Contours from MOLA data are in kilometers, see Fig. 10 for location. "R" identifies a wrinkle ridge which most likely formed by the deformation of the patera floor. Black arrows point to lava flow lobes which appear to travel up-slope. Mosaic of CTX frames B06_012006_1912 and B07_012362_1912.

Table 1

Estimated volumes of the individual patera within the Olympus Mons caldera. These volumes assume that each collapse event formed an elliptical or circular depression, and that the elevation of the rim of each patera relative to the elevation of the foot of the wall has not been influenced by the inflation of the summit. In part, Apollo, Athena and Dionysus paterea overlap older collapse events, and so two values for the volume change are given.

Patera	Area (km^2)	Ht. drop (km)	Vol. (km^3)	Total volume (km^3)
Apollo	125	3.0	375	
Apollo	125	0.3	37	412
Athena	125	1.8	225	
Athena	200	1.0	200	425
Dionysus	157	0.8	126	
Dionysus	157	2.5	392	518
Hera	330	1.4	462	462
Hermes	1250	0.6	750	750
Zeus	2827	1.3	3,675	3,675

Total Volume = 6,242 km^3

Table 2

Dimensions of the Aganippe Fossa and Phoenicis graben. Values in parentheses are influenced by local collapse and enlargement of the surface depressions and are unreliable indicators of dike geometry. See Fig. 8 for profile locations.

(a) Aganippe Fossa

location	graben width/km	graben depth/m	dike width/m	dike top depth/km
1	11.5	220	280	3.3
2	12.3	340	425	3.5
3	7.0	550	690	2.0
4	6.2	640	800	1.8
5	5.2	290	360	1.5
6	2.9	210	265	0.8
7	(8.4)	(960)	(1200)	(2.4)
8	(17.6)	(1540)	(1930)	(5.0)
9	(7.9)	(910)	(1140)	(2.3)
10	7.1	140	180	2.0

(b) Phoenicis graben

location	graben width/km	graben depth/m	dike width/m	dike top depth/km
1	(10.2)	(2240)	(2800)	(2.9)
2	(11.0)	(1890)	(2365)	(3.1)
3	3.5	545	680	1.0
4	3.2	615	770	0.9
5	5.9	430	540	1.7
6	4.5	250	310	1.3
7	5.3	70	85	1.5
8	3.4	210	265	1.0
9	3.3	115	145	0.9